

Measurement and modeling of three-dimensional equilibria in DIII-D

M. J. Lanctot, H. Reimerdes, A. M. Garofalo, M. S. Chu, J. M. Hanson et al.

Citation: *Phys. Plasmas* **18**, 056121 (2011); doi: 10.1063/1.3593009

View online: <http://dx.doi.org/10.1063/1.3593009>

View Table of Contents: <http://pop.aip.org/resource/1/PHPAEN/v18/i5>

Published by the [American Institute of Physics](#).

Related Articles

Production of internal transport barriers via self-generated mean flows in Alcator C-Mod
Phys. Plasmas **19**, 056113 (2012)

Collision frequency dependence of polarization current in neoclassical tearing modes
Phys. Plasmas **19**, 032120 (2012)

Observation of the generation and evolution of long-lived runaway electron beams during major disruptions in the HuanLiuqi-2A tokamak
Phys. Plasmas **19**, 032510 (2012)

Comparison of anomalous Doppler resonance effects with molybdenum and graphite limiters on HT-7
Phys. Plasmas **19**, 032509 (2012)

Control of post-disruption runaway electron beams in DIII-D
Phys. Plasmas **19**, 056109 (2012)

Additional information on *Phys. Plasmas*

Journal Homepage: <http://pop.aip.org/>

Journal Information: http://pop.aip.org/about/about_the_journal

Top downloads: http://pop.aip.org/features/most_downloaded

Information for Authors: <http://pop.aip.org/authors>

ADVERTISEMENT



HAVE YOU HEARD?

Employers hiring scientists
and engineers trust
physicstodayJOBS



<http://careers.physicstoday.org/post.cfm>

Measurement and modeling of three-dimensional equilibria in DIII-D^{a)}

M. J. Lanctot,^{1,b),c),d)} H. Reimerdes,^{1,e)} A. M. Garofalo,² M. S. Chu,² J. M. Hanson,³
 Y. Q. Liu,⁴ G. A. Navratil,¹ I. N. Bogatu,⁵ Y. In,⁵ G. L. Jackson,² R. J. La Haye,²
 M. Okayabashi,⁶ J.-K. Park,⁶ M. J. Schaffer,² O. Schmitz,⁷ E. J. Strait,² and A. D. Turnbull²

¹Department of Applied Physics and Applied Mathematics, Columbia University,
 New York, New York 10027, USA

²General Atomics, P.O. Box 85608, San Diego, California 92186-5608, USA

³Oak Ridge Institute for Science and Education, P.O. Box 117, Oak Ridge, Tennessee 37831-0117, USA

⁴EURATOM/UKAEA Fusion Association, Culham Science Centre, Abingdon, Oxfordshire OX14 3DB,
 United Kingdom

⁵FAR-TECH, Inc., San Diego, California 92121, USA

⁶Princeton Plasma Physics Laboratory, Princeton, New Jersey 08543-0451, USA

⁷Institut für Energieforschung-Plasmaphysik, Forschungszentrum Julich GmbH, EURATOM Association,
 Trilateral Euregio Cluster, D-52425 Julich, Germany

(Received 18 January 2011; accepted 2 May 2011; published online 31 May 2011)

A detailed experiment-theory comparison reveals that linear ideal MHD theory is in quantitative agreement with external magnetic and internal soft x-ray measurements of the plasma response to externally applied non-axisymmetric fields over a broad range of beta and rotation. This result represents a significant step toward the goal of advancing the understanding of three-dimensional tokamak equilibria. Both the magnetic and soft x-ray measurements show the driven plasma perturbation increases linearly with the applied perturbation, suggesting the relevance of linear plasma response models. The magnetic and soft x-ray measurements are made at multiple toroidal and poloidal locations, allowing well resolved measurements of the global structure. The comparison also highlights the need to include kinetic effects in the MHD model once beta exceeds 80% of the kink mode limit without a conducting wall. Two distinct types of response fields are identified by the linear ideal MHD model: one that consists of localized currents at the rational surfaces that cancel the applied resonant field and another that is excited by the components of the external field that couple to the kink mode. Numerical simulations show these two fields have similar amplitudes in ITER-shaped DIII-D discharges where $n = 3$ fields are used to suppress edge localized modes. © 2011 American Institute of Physics. [doi:10.1063/1.3593009]

I. INTRODUCTION

Non-axisymmetric (3D) magnetic fields are used in the DIII-D tokamak¹ to extend the operational space and improve plasma performance. For example, currents in external non-axisymmetric coils, such as the internal coil (I-coil),² are used to modify the non-axisymmetric magnetic field (or error field) that exists due to unavoidable departures from axisymmetric geometry.^{3–5} Determining the optimal currents is crucial especially at high normalized plasma beta, $\beta_N = \beta_t(aB/I_p)$,⁶ and low density.⁷ Here $\beta_t = 2\mu_0\langle p \rangle/B_t^2$, $\langle p \rangle$ is the volume averaged plasma pressure, B_t is the total on-axis toroidal magnetic field, a is the plasma minor radius, and I_p is the total plasma current. Non-axisymmetric magnetic fields have also been used to suppress edge localized modes (ELMs),^{8,9} instabilities in the edge transport barrier of high-confinement (H-mode) tokamak plasmas that result in potentially damaging bursts of heat and particle flux into the scrape-off region and onto the divertor. ELM suppression

techniques are urgently needed in future machines that will require the good energy confinement of H-mode. Non-axisymmetric fields with dominantly non-resonant components can also drive or slow the plasma rotation, which is known to affect the plasma stability and resilience to error fields.¹⁰ In order to develop robust control methods using 3D fields, an improved theoretical and empirical understanding of the 3D magnetic topology in tokamaks is needed.

In 3D toroidal devices, non-axisymmetric shaping is the fundamental design parameter used to provide robust passive plasma control and minimize neoclassical transport.¹¹ To calculate the magnetic topology in these configurations, the ideal MHD force balance equation must be solved since no general simplification exists.¹² The lack of axisymmetry means that closed equilibrium flux surfaces are not guaranteed to occur. In a helical equilibrium, the lowest energy state may include magnetic islands, which if large enough can overlap to form ergodic regions. While 3D fields exist also in tokamaks, the total 3D magnetic field $\delta\vec{B}^{tot}$ is small compared to the axisymmetric magnetic field \vec{B}_0 . In this work, $\delta\vec{B}^{tot}/B_0 < 10^{-3}$. This suggests linear perturbation theory may be used to find the non-axisymmetric equilibrium consistent with force balance.^{13,14} This approach uses the axisymmetry of the tokamak to reduce the force balance equation to the Grad-Shafranov equation, which can be solved using codes such as EFIT

^{a)}Paper BI3 2, Bull. Am. Phys. Soc. 55, 23 (2010).

^{b)}Invited speaker.

^{c)}Electronic mail: lanctot1@llnl.gov.

^{d)}Present address: Lawrence Livermore National Laboratory, 7000 East Ave., Livermore, California 94550, USA.

^{e)}Present address: CRPP-EPFL, CH-1015 Lausanne, Switzerland.

(Ref. 15) to obtain the poloidal flux function describing closed, nested flux surfaces. Then, codes such as MARS-F¹⁶ or IPEC (Ref. 17) can be used to find the non-axisymmetric equilibrium, which includes externally applied non-axisymmetric magnetic fields ($\delta\vec{B}^{ext}$) and the plasma response ($\delta\vec{B}^{plas}$), which is the component of the magnetic field generated by currents inside the plasma.

This paper describes efforts to validate models of non-axisymmetric equilibria using measurement of the plasma response in DIII-D and plasma response calculations with the MARS-F code. MARS-F solves the linearized single-fluid MHD equations including plasma resistivity and rotation. The model includes the geometry of the external non-axisymmetric coils and an axisymmetric resistive wall. First, we demonstrate that linear ideal MHD theory describes the measured magnetic plasma response field in rotating discharges below the ideal MHD no-wall limit ($\beta_N^{no-wall}$), which is the predicted ideal MHD pressure limit without a conducting wall near the plasma surface. A measure of the internal structure of the $n=1$ plasma response derived from toroidally distributed soft x-ray measurements shows an ideal MHD structure, with an amplitude that increases linearly with the applied perturbation strength. Quantitative agreement between the measurements and a model of the perturbed soft x-ray signals is demonstrated. Next, modeling of the $n=3$ structure of $\delta\vec{B}^{plas}$ underscores there are two types of ideal MHD response fields: one that consists of localized currents at the rational surfaces that cancel the applied resonant field and another that is excited by the components of the external field that couple to the kink mode. MARS-F calculations predict these two response fields have similar amplitudes in ITER-shaped DIII-D discharges where $n=3$ fields are used to suppress edge localized modes.

II. PLASMA RESPONSE MEASUREMENT TECHNIQUES

Non-axisymmetric plasma equilibria are created in the DIII-D tokamak using the I-coil, a set of 12 picture-frame coils located above and below the midplane. The I-coil can apply an external field with a range of toroidal and poloidal mode numbers n and m . External fields with $n=1$ and $n=3$ have been used to probe rotating H-mode discharges heated by neutral beam injection (NBI). For $n=1$ studies, the poloidal mode spectrum of the external field is determined by the I-coil phase difference ($\Delta\phi$), which is the toroidal phase shift between the currents in the upper and lower I-coil arrays. When applying $n=3$ magnetic perturbations, the poloidal mode spectrum is controlled by the “parity”. The even parity field is up-down symmetric, while the odd parity field is up-down anti-symmetric. Step I-coil current waveforms were used to measure the $n=3$ plasma response,¹⁸ while slowly rotating fields were used to probe discharges with $n=1$ fields.¹⁹

It is important to appreciate the relevant time scales in these experiments. Following a change in either the axisymmetric and non-axisymmetric coil currents, ideal MHD force balance is restored on the Alfvén time scale, which is less than 10^{-7} s. Throughout the discharge, the plasma current profile continues to evolve since the duration of the current

flattop is on the order of the resistive diffusion time, which is a few seconds. There is no conflict between this evolution and force balance since the plasma passes through neighboring equilibria.²⁰ In experiments using $n=1$ and $n=3$ fields, the perturbations are essentially static since the time scale for changes in the coil currents, 10^{-2} to 10^{-1} s, is long compared to the inverse plasma rotation frequency of 10^{-5} to 10^{-4} s. Eddy currents in the wall do act to reduce the amplitude of a rotating $n=1$ field particularly when the field rotation frequency, f_{ext} , exceeds a few hundred hertz. This is because the time for flux diffusion through the resistive vacuum vessel wall is on the order of 10^{-3} s. However, for $f_{ext}=10$ Hz, there is little attenuation of the field. Nevertheless, the effect of the eddy currents is accounted for in MARS-F, which models both static and time-varying external fields.

The non-axisymmetric magnetic field is detected using toroidal arrays of poloidal field probes and saddle loops. Typically, the midplane poloidal field probes ($\delta B_{p,mid}$) and the midplane radial field probes ($\delta B_{r,mid}$) are closest to the plasma surface; hence, they are most sensitive to the plasma response, which is obtained by subtracting the known coil-sensor coupling from the total perturbed field. The internal perturbation structure is measured using a soft x-ray imaging system, which consists of three 12-channel systems viewing poloidal cross-sections of the plasma at three separate toroidal locations.²¹ The hardware was recently refurbished and calibrated to enhance the sensitivity to $n=1$ perturbations.

Fourier analysis and spatial fitting of the I-coil currents, the magnetic sensor signals, and the soft x-ray signals are used to determine the $n=1$ response amplitudes, Fig. 1. Here, a complex notation δB_s^n is used for the mode components of a toroidal array s , with $\delta B(\phi) = \text{Re}[\delta B_s^n e^{-in\phi}]$ recovering the

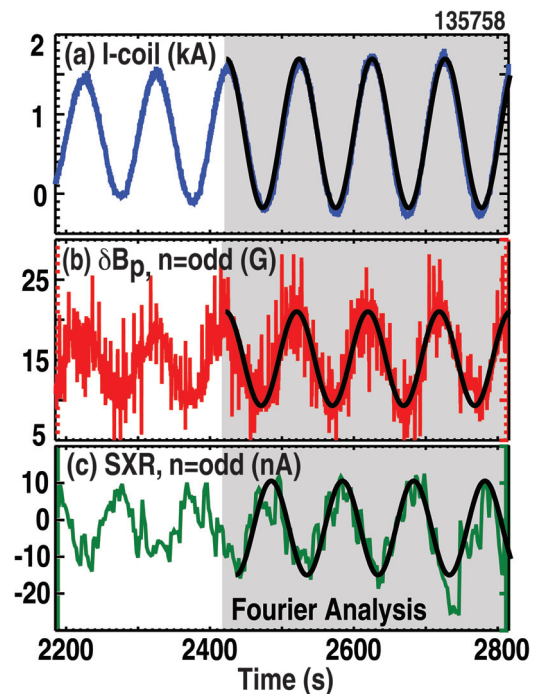


FIG. 1. (Color online) Time trace of (a) the current in the I-coil, and the $n=1$ amplitude of (b) $\delta B_{p,mid}^{plas}$, and (c) a soft x-ray channel near the plasma edge for discharge 135758. Fourier analysis (solid black trace) is used to extract the plasma response amplitude.

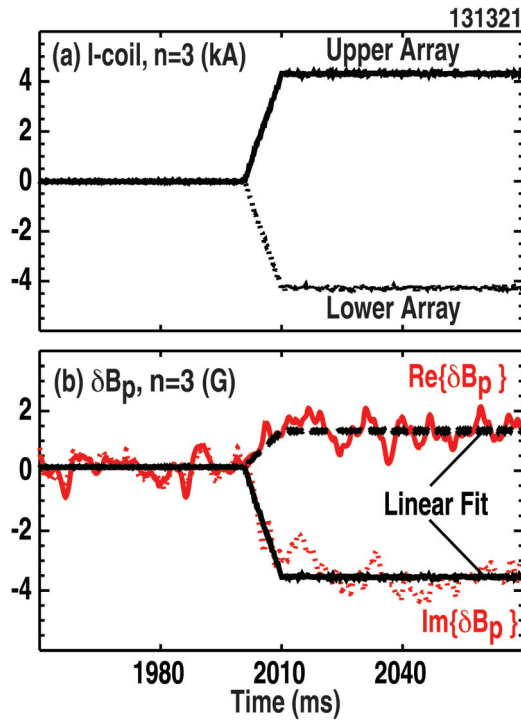


FIG. 2. (Color online) Time trace of the $n=3$ amplitude of (a) the current in the I-coil and (b) $\delta\vec{B}_{p,\text{mid}}^{\text{plas}}$ in discharge 131321. The solid and dashed black lines show the linear fit used to determine the plasma response amplitude.

signal at a toroidal angle ϕ . To analyze the $n=3$ magnetic measurements, the complex $n=3$ amplitude is extracted from the midplane poloidal field array and linear regression is used to fit the real and imaginary parts with the $n=3$ I-coil current amplitude as the independent variable, Fig. 2.

III. TESTS OF THE LINEAR IDEAL MHD PERTURBED EQUILIBRIUM MODEL

Previous measurements in DIII-D have shown that the magnetic plasma response is linear in the external field amplitude.²² Recent experiments also confirmed the linearity of the internal response. In 135762, the amplitude of a rotating (10 Hz) $n=1$ I-coil field was ramped between 1.0 and 2.0 kA at $\beta_N = 1.4$. A linear response is observed in the magnetic measurements, shown here for the poloidal and radial plasma response measurements at the midplane, $\delta\vec{B}_{p,\text{mid}}^{\text{plas}}$ and $\delta\vec{B}_{r,\text{mid}}^{\text{plas}}$, Fig. 3. The plasma response measured by the soft x-ray diagnostic ($\delta s/s_0$) also exhibits a linear dependence, which is shown for a channel with a tangency radius near $\psi \sim 0.82$. Here, δs is the $n=1$ soft x-ray amplitude, s_0 is the equilibrium or $n=0$ amplitude, and ψ is the normalized poloidal flux. It is useful to normalize the $n=1$ soft x-ray amplitude by the $n=0$ amplitude since the dc signal level can change significantly during a discharge. The observed linear dependence is expected to breakdown when the non-axisymmetric field becomes sufficiently large; however, in DIII-D, this state is typically preceded by a collapse of the plasma rotation and the formation of a locked magnetic island.²³

In rotating discharges below the no-wall beta limit, the measured plasma response amplitude is in good agreement with the linear ideal MHD model in MARS-F in which the

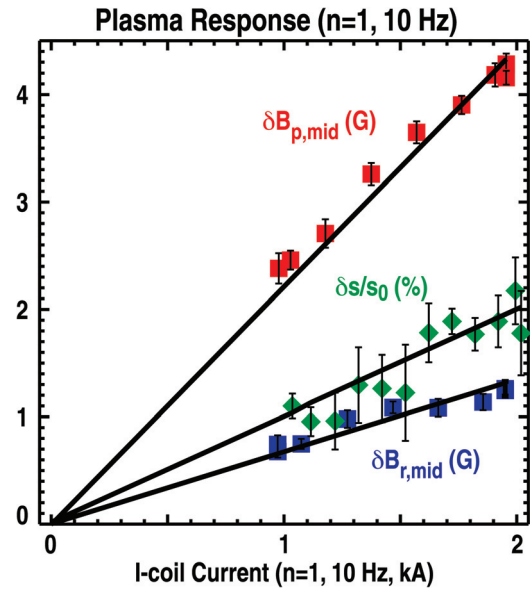


FIG. 3. (Color online) Dependence of the $n=1$ plasma response on the applied I-coil current as measured by $\delta B_{p,\text{mid}}$, $\delta B_{r,\text{mid}}$, and an edge channel of the soft x-ray array ($\delta s/s_0$). The solid lines represent linear fits constrained to pass through the origin.

plasma rotation and resistivity were set to zero. This was demonstrated in experiments where at $t=2$ s, the $n=1$ I-coil current amplitude was ramped up to 4.7 kA at $t=3$ s. Figure 4(a) shows the evolution of the plasma rotation near the $q=2$ surface, which decreases and finally collapses at $t \sim 2.9$ s. Prior to the collapse, the plasma response amplitude was linear in the I-coil current, independent of rotation, Fig. 4(b), and is in good agreement with MARS-F calculations. One objection to this type of MARS-F calculation is that it excludes the plasma rotation, which, experimentally, is required to prevent the formation of a magnetic island in the presence of a pitch resonant external field. As this comparison shows, it is not necessary to explicitly model the rotation since the initial closed flux surface topology is maintained in code not by the rotation but by the ideal MHD constraint. The implication is that in the experiment the rotation

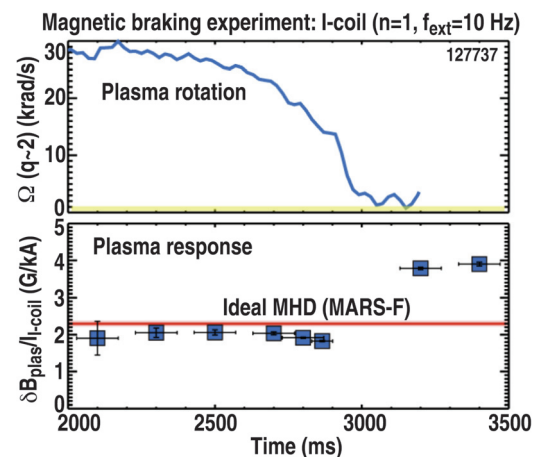


FIG. 4. (Color online) (Top) Time evolution of the plasma rotation near the $q=2$ during an experiment where the $n=1$ I-coil current amplitude is ramped starting at 2 s. (Bottom) Comparison of the measured $n=1$ amplitude of $\delta\vec{B}_{p,\text{mid}}^{\text{plas}}$ with the value predicted by MARS-F.

was large enough to completely screen out the resonant field. Following the rotation collapse, the plasma response deviates from the linear ideal MHD model and the formation of a magnetic island is observed (Fig. 2 in Ref. 23). In order to model the plasma response in this case where there is incomplete screening of external fields, the plasma rotation and resistivity must be included self-consistently.

All the plasma response measurements reported below were made in discharges where the plasma rotation was maintained by co-NBI. It is important to keep in mind that in these experiments, the external fields are applied for times between 10^{-1} and 1 s, which is much longer than a reconnection time, τ_{rec} . An estimate for τ_{rec} of 10^{-3} to 10^{-2} s at the resonant magnetic surfaces was calculated using the theory of Fitzpatrick.²⁴ We conclude that the resulting state satisfies the requirements for a three-dimensional plasma equilibrium, which is free of islands driven by the externally applied field, i.e., there is no driven magnetic reconnection. As shown above, this state persists provided the plasma rotation frequency exceeds τ_{rec}^{-1} .

Plasma response measurements were used to test the linear ideal MHD perturbed equilibrium model over a range of β_N . As described in Ref. 25, reconstructions of the 2D plasma equilibrium and plasma response calculations were done for 5 discharges where $1.1 < \beta_N < 2.0$. For each discharge, magnetic field pitch angle measurements from multiple motional Stark effect (MSE) polarimeters,²⁶ kinetic profile measurements from Thomson scattering²⁷ and charge exchange recombination spectroscopy (CER),²⁸ and ONETWO (Ref. 29) transport calculations of the total pressure, including the contribution from non-thermal beam ions, were used to constrain reconstructions of the axisymmetric magnetic field using the EFIT code. The equilibria were used as input to the MARS-F code to calculate the plasma response and predict the sensor signals. Figure 5 shows good agreement between the measured plasma response amplitude and phase and the predicted sensor signals for a discharge at $\beta_N = 1.4$. The phase is quoted with respect to the applied radial field at the midplane. The measurements reveal that the

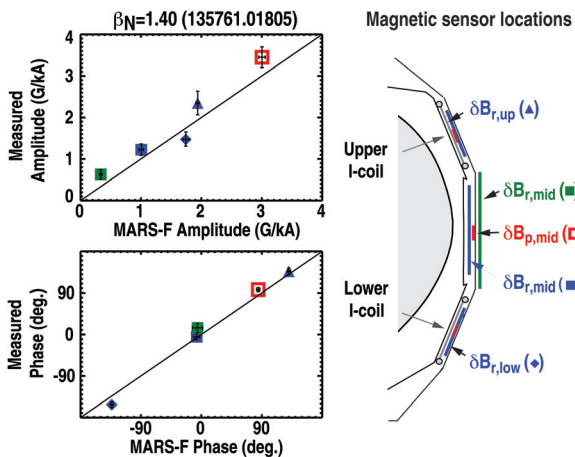


FIG. 5. (Color online) (Left) Comparison of the measured $n = 1$ amplitude and phase of $\delta B_{p, \text{mid}}^{\text{plas}}$ at multiple poloidal locations with the signals predicted by MARS-F. (Right) Locations of the upper and lower I-coil arrays, poloidal field probes, and saddle loop coils.

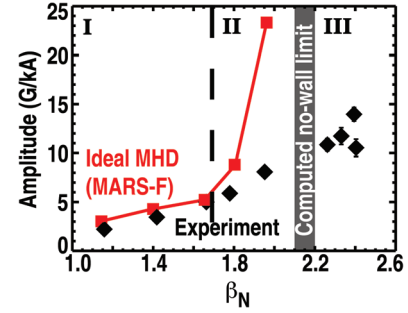


FIG. 6. (Color online) Comparison of the measured $n = 1$ amplitude of $\delta B_{p, \text{mid}}^{\text{plas}}$ (black diamonds) with the signals predicted by MARS-F (red squares) as a function of β_N . The vertical grey bar marks the computed no-wall limit.

perturbation is in phase with δB^{ext} , and the phase of $\delta B_{p, \text{mid}}^{\text{plas}}$ is shifted $+90^\circ$ in the co- I_p direction from $\delta B_{r, \text{mid}}^{\text{plas}}$.

The ideal MHD model is adequate to describe the plasma response for $\beta_N < 1.8$ where the amplitude of $\delta B_{p, \text{mid}}^{\text{plas}}$ exhibits a linear dependence on β_N (region I in Fig. 6). At pressures approaching the ideal MHD no-wall limit (region II), the linear ideal MHD model gradually overestimates the response amplitude, and the calculated amplitude becomes increasingly sensitive to the details of the equilibrium profiles, particularly, the amount of edge bootstrap current, which has an effect on the internal inductance and the no-wall beta limit. The sensitivity of the predicted plasma response amplitude to the resistivity of the vacuum vessel wall was also checked. By increasing the wall time (or decreasing the wall resistivity) a factor of 10 over the experimental value ($\tau_{\text{wall}} \approx 3$ ms for a $n = 1$ eigenmode in DIII-D), the amplitude of $\delta B_{p, \text{mid}}^{\text{plas}}$ can be reduced by 4 G/kA. The amplitude is reduced below the 1 G/kA in the presence of an ideal conducting wall due to wall eddy currents that affect the stability beta limits and the externally applied field. Above the no-wall limit (region III), the ideal MHD model predicts instability, while the experiment remains stable. In this regime, 3D equilibrium measurements have been shown to be consistent with kinetic resistive wall mode (RWM) stability models.³⁰ We speculate that kinetic effects are also modifying the plasma stability below the no-wall beta limit.

The measured internal structure of the driven perturbation derived from toroidally distributed soft x-ray measurements³¹ has been compared for the first time with the linear ideal MHD model. A model for the equilibrium and $n = 1$ soft x-ray measurements was developed for this purpose. It assumes that the equilibrium emissivity (S) is dominated by thermal bremsstrahlung and is constant on a poloidal flux surface. Accordingly, an emissivity function of the form

$$G(E, \psi) = p_0 n_e(\psi) n_i(\psi) Z_i^2 \frac{e^{-E/T_e(\psi)}}{\sqrt{T_e(\psi)}} \quad (1)$$

was employed. Here, $E = h\nu$, h is Planck's constant, ν is the radiation frequency, Z_i is the ion charge, and p_0 is an empirically determined calibration coefficient, which can be found by cross-calibrating the soft x-ray measurements against the thermal electron density (n_e), electron temperature (T_e), and ion

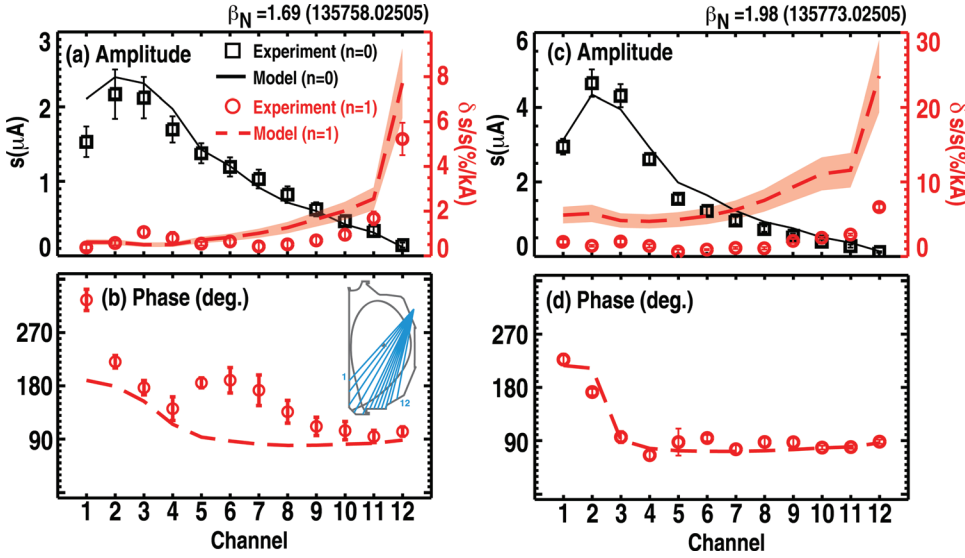


FIG. 7. (Color online) Comparisons of (a), (c) (left ordinate) the measured (black squares) and simulated (solid black line) $n=0$ soft x-ray amplitude, (right ordinate) the measured (red circles) and simulated (dashed red line) $n=1$ soft x-ray amplitude. (b), (d) Comparison of the measured (red circles) and simulated (dashed red line) $n=1$ phase. Results are shown for two cases: (a), (b) $\beta_N = 1.69$ (135758 at 2505 ms) and (c), (d) $\beta_N = 1.98$ (135773 at 2505 ms). The inset in (b) shows the sightline geometry.

density (n_i) measurements. Only the thermal deuterium ion and carbon VI impurity ion densities were considered; fast ions and other impurities were neglected. The spectral filter-detector responsivity (η) is modeled using $\eta = e^{-\mu_{Be}l_{Be}} \times (1 - e^{-\mu_d l_d})$. The known thicknesses (l_{Be} , l_d) of the beryllium filters and the silicon photodiode arrays are used. The photoabsorption coefficients (μ_{Be} , μ_d) are taken from a NIST database.³² When computing the equilibrium emission, the expression

$$S_0(\psi) = \int_E G(E, \psi) \eta(E) dE \quad (2)$$

is numerically integrated on each ψ contour for a given equilibrium. The result is interpolated onto an EFIT grid. For each chord, the spatial calibration is used to construct a mask, which when multiplied with $S_0(R, Z)$ gives the integrand of the volume integral. A Gaussian weighting scheme is used for points inside the observation region to account for the finite size of the slit aperture and detector, and the measured instrument response. The i_{th} soft x-ray measurement, s_i , is obtained by summing the integrand together with the differential volume element

$$s_i = \frac{w_a A_d \cos \theta}{4\pi d} \int_{\Omega} \frac{S_0(R, Z)}{\sqrt{(R - r_i)^2 + (Z - z_i)^2}} dR dZ, \quad (3)$$

where w_a is the width of the aperture, A_d is the area of the detector, θ is the angle between the normal vector to the detector surface and the line of sight, d is the detector-aperture distance, and (r_i, z_i) is the center of the i_{th} detector element. The perturbed equilibrium signals are calculated in a similar way using a perturbed emissivity, $\delta S(\psi)$, based on the assumption that the emissivity is convected with the mode displacement, $\delta S(\psi) = -\xi \cdot \nabla S = -\xi \cdot \nabla \psi \partial S / \partial \psi$. The model uses the normal component of the displacement (with units of meters per kA) calculated using MARS-F.

The model is in quantitative agreement with the measured $n=1$ soft x-ray signal over the range of β_N where

MARS-F agrees with the measured $n=1$ magnetic fields. Figures 7(a) and 7(b) show a comparison of the $n=0$ and the $n=1$ soft x-ray measurements with the simulated signals at $\beta_N = 1.69$ (135758 at 2505 ms). The modeled $n=0$ soft x-ray profile agrees with the measured profile, indicating that bremsstrahlung is the dominant source of radiation in this case. In the model, the parameter p_0 was adjusted to best match the $n=0$ signal amplitude. The measured $n=1$ $\delta s/s_0$ is also reproduced by the model, which shows the perturbed amplitude is largest near the plasma edge (channel 12). It is important to note that the value of p_0 does not affect $\delta s/s_0$. The shaded region represents an estimate of the error in the predicted amplitude due to variations in the gradient of the simulated soft x-ray emissivity. The error is less than 20% for variations in the electron density, electron temperature, and carbon impurity density profiles within the experimental uncertainties.

The simulated and measured phases are in very good agreement near the plasma edge, where $\delta s/s_0$ is the largest, Fig. 7(b). However, for channels 5-9, the measured phase is shifted in the direction of the plasma current and rotation by as much as 100°. This shift is not the signature of a magnetic island at the frequency of the applied magnetic field. If such an island was present, there would be a 180° shift localized near the mode rational surface. In this discharge, small amplitude tearing modes were observed on the magnetic diagnostics, but at frequencies >35 kHz. Since this is well above the frequency of the driven perturbation (10 Hz), the tearing modes are not expected to interact with the plasma response. Rather, the discrepancy in the phase results because the signal-to-noise level of δs is small so that the phase is not well defined. This is supported by the observed increase in the error bars for those channels.

Comparisons between the measured and simulated soft x-ray measurements made in discharges at lower values of β_N show similar or better agreement. However, as β_N increases toward the $n=1$ no-wall limit, the ideal plasma model overestimates the internal perturbation amplitude as expected from the analysis of the magnetic measurements.

Figures 7(c) and 7(d) show a comparison at $\beta_N = 1.98$ (135773 at 2505 ms) where the model overestimates the edge amplitude by a factor of 3.5. The singular dependence of the plasma response amplitude near the no-wall limit occurs because the ideal plasma model is missing the correct damping terms, which, if included, would stabilize the RWM. Interestingly, the measured and modeled phase of the plasma response are in excellent agreement. This confirms the absence of any large scale driven magnetic reconnection and indicates that the mechanisms responsible for modifying the amplitude of the plasma response do not change the phase in this range of β_N .

IV. TWO TYPES OF RESPONSE FIELDS

In the linear ideal MHD model, two types of non-axisymmetric fields are associated with the plasma response: the pitch resonant field and the field associated with the global kink mode. These fields can be characterized using a straight field line coordinate system. Of interest is $\delta B_{r(m,n)}$, the radial component of δB associated with the Fourier harmonics (m, n) (Appendix A of Ref. 33). The pitch resonant fields are the harmonics satisfying $m = nq$ at the rational surfaces. In an ideal conducting plasma, the application of an external resonant field leads to the induction of localized currents that exactly cancel the resonant component of the external field. External fields can also couple to the global kink mode, which is an ideal MHD instability with extensive poloidal mode coupling.

Above the no-wall limit, the growth rate of the kink mode can be slowed by the presence of a conducting wall located near the plasma boundary, but the mode cannot be stabilized if the wall has finite conductivity.³⁴ The slowly growing instability is referred to as the RWM, which has a structure similar to the kink mode [Fig. 7(a) of Ref. 23]. The poloidal harmonics of the kink mode are largest in the spectral region of $|m| > |nq|$. (The sign of m and q depends on the direction of the toroidal magnetic field and the plasma current.) The eigenmodes associated with the screening of the resonant field and the kink mode form a set of plasma modes each described by a plasma fluid displacement, perturbed plasma current, perturbed magnetic field, and complex frequency representing the mode growth rate and rotation frequency.³⁵ When the growth rate is negative, the mode is damped but can be excited by external fields that couple to the eigenmode.

Linear ideal MHD calculations with MARS-F suggest that the $n = 3$ odd parity I-coil field primarily drives a plasma response field that couples to the kink mode in lower single-null equilibria with an upper triangularity δ_u of 0.1, on-axis safety factor $q_0 > 1.0$, and $q_{95} = 5.0$ [q_{95} is the safety factor at the 95% normalized poloidal flux surface]. Figure 8(a) shows the poloidal spectrum of the odd parity $n = 3$ $\delta B_{r(m,n)}$ in vacuum. There is a spectral valley near the locus of points satisfying $m = nq$ and a peak in the kink mode region of the spectrum. These components excite the kink mode in the presence of a plasma, shown in Fig. 8(b) for a case where

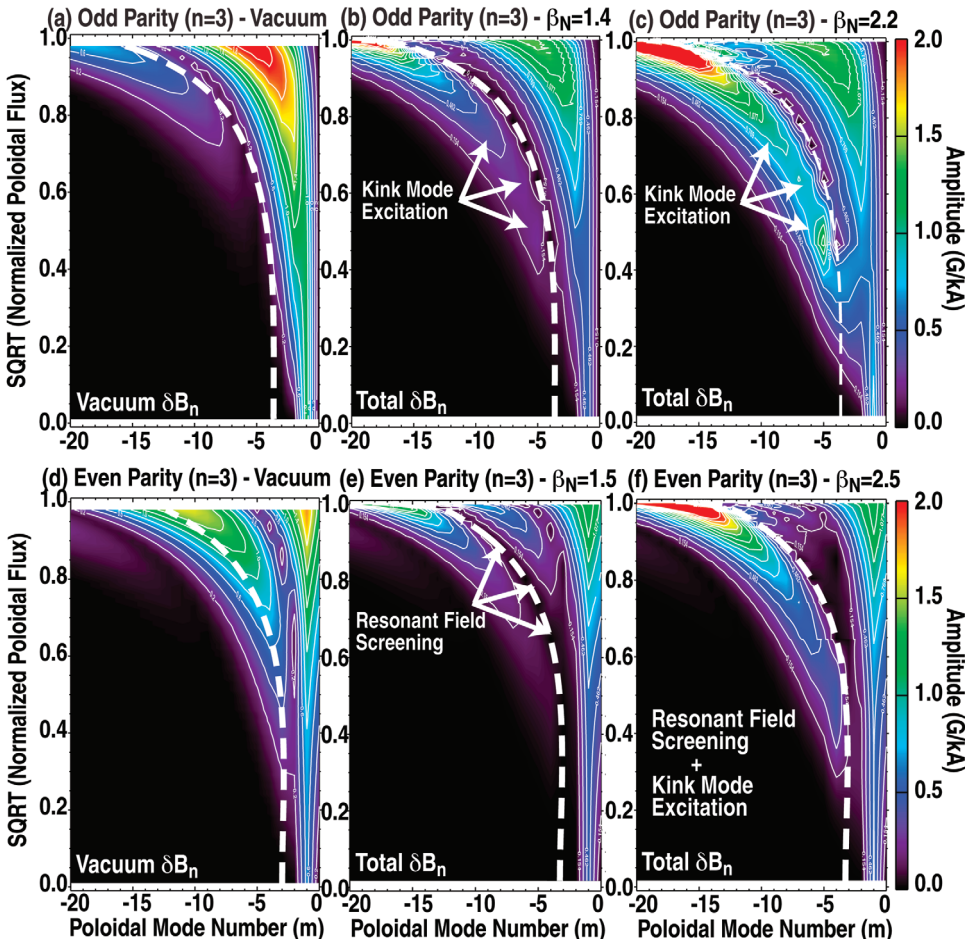


FIG. 8. (Color) Amplitudes of the $n = 3$ poloidal mode harmonics of $\delta B_{r(m,n)}$ calculated with MARS-F as a function of $\sqrt{\psi}$. (top row) Spectra of the odd parity configuration: (a) without plasma, (b) total field with plasma ($\beta_N = 1.4$), and (c) total field with plasma ($\beta_N = 2.4$). (bottom row) Spectra for the even parity configuration: (d) without plasma, (e) total field with plasma ($\beta_N = 1.5$), and (f) total field with plasma ($\beta_N = 2.5$). The dashed white line marks the locus of points satisfying $m = nq$.

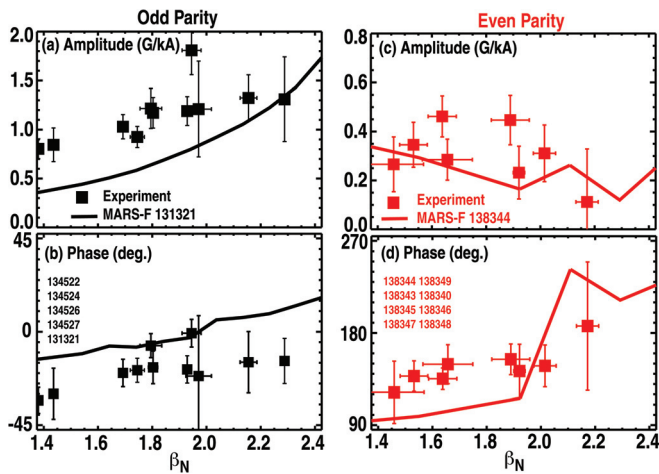


FIG. 9. (Color online) Comparison of the measured amplitude (top) and phase (bottom) of the $n=3$ plasma response ($\delta\vec{B}_{p,mid}^{plas}$) with the signals predicted by MARS-F as a function of β_N for I-coil fields with (a), (b) odd and (c), (d) even parity.

$\beta_N = 1.4$. The kink type response increases with β_N , Fig. 8(c). In discharges with a poloidal shape similar to the ITER baseline scenario (lower single null and $\delta_u = 0.32$) and $q_{95} = 4.0$, the even parity I-coil field has strong pitch resonant components, Fig. 8(d). However, these components are screened in the presence of a plasma, Fig. 8(e). The screening field is constant as β_N increases while the kink mode components contribute an increasing fraction of the total radial field, Fig. 8(f).

The measured $n=3$ plasma response to odd and even parity I-coil fields is consistent with the linear ideal MHD model. When odd parity I-coil fields are applied to rotating H-mode discharges, the measured $\delta\vec{B}_{p,mid}^{plas}$ increases monotonically over the explored range of β_N in good agreement with MARS-F calculations, Figs. 9(a) and 9(b). In contrast, the measured $\delta\vec{B}_{p,mid}^{plas}$ decreases with β_N when even parity fields are applied, which is also captured by the model, Figs. 9(c) and 9(d). The calculations use an input scaled pressure equilibria based on a single kinetic equilibrium reconstruction calculated from each of the two target discharges: 131321 (odd parity) and 138344 (even parity).

Compared to the $n=1$ experimental results, there is an increase in the deviations between the measured $n=3$ plasma response and the linear ideal MHD model. This increase with higher toroidal mode number is not unexpected since the plasma stability and the plasma response amplitude increasingly depends on the state of the pressure profile within the ELM cycle. This dependence on the details of the pressure profile evolution was not captured in the present plasma response modeling, which used equilibrium reconstructions constrained by pressure profile measurements that were averaged over many ELM cycles, and was taken at random times during an ELM cycle. Analysis of the pressure profile evolution during an ELM is needed to quantify the sensitivity of the plasma response to these changes.

The unexpected β_N dependence of the $n=3$ plasma response to the even parity field prompted a numerical study in ITER-shaped DIII-D equilibria using modified equilibria

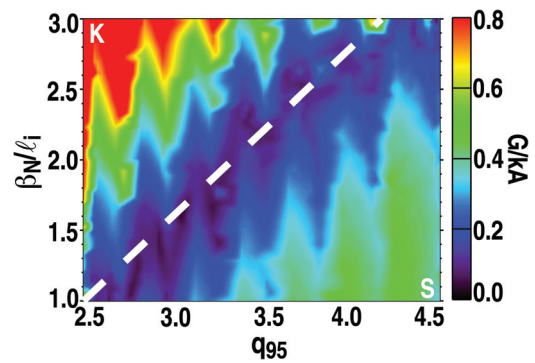


FIG. 10. (Color) Amplitude of the $n=3$ $\delta\vec{B}_{p,mid}^{plas}$ calculated by MARS-F for the even parity I-coil configuration as a function of β_N/ℓ_i and q_{95} . The dashed white line guides the eye to where the amplitude attains a minimum value.

based on 138344. The Grad-Shafranov solver in the CORSICA code³⁶ was used to construct equilibria with plasma parameters: $1.0 < \beta_N/\ell_i < 3.0$, $2.5 < q_{95} < 4.5$, and $q_0 \sim 1.05$. It is important to hold β_N/ℓ_i fixed while varying q_{95} since the no-wall beta limit is known to scale with ℓ_i , the plasma internal inductance.³⁷ MARS-F was used to calculate the linear ideal MHD plasma response for over 1000 equilibria in this range of plasma pressure and plasma current, which includes the parameter space where $n=3$ even parity fields have been used to suppress ELMs in DIII-D: $1.5 < \beta_N/\ell_i < 2.5$ and $q_{95} = 3.6 \pm 0.2$.³⁸

The predicted amplitude of the $n=3$ $\delta\vec{B}_{p,mid}^{plas}$ is found to depend not only on β_N but also on the safety factor, Fig. 10. At $q_{95} = 4.5$, the plasma response decreases with β_N/ℓ_i , while the opposite trend is observed at $q_{95} = 2.5$. For intermediate values of q_{95} , the amplitude decreases with β_N/ℓ_i , attains a minimum value (marked by the dashed white line), and then increases. The phase of the plasma response (not shown) shifts most rapidly (by $\sim 90^\circ$) across the region where the amplitude reaches a minimum, as in Fig. 9(d). In the region of Fig. 10 marked ‘‘S’’ (for screening), the poloidal spectrum of the total $\delta B_{r(m,n)}$ has a structure like Fig. 8(e) while in the region marked ‘‘K’’ (for kink), the structure is similar to Fig. 8(f). These trends are observed only at the midplane. At off-midplane locations, the plasma response increases monotonically as the plasma pressure and plasma current increase. The implications of this result for ELM suppression by external fields are presently being explored.

V. SUMMARY

In summary, we have shown that the linear ideal MHD plasma response model in the MARS-F code is in quantitative agreement with the measured $n=1$ and $n=3$ magnetic plasma response in rotating H-mode plasmas provided the plasma is below 80% of the no-wall beta limit. The internal $n=1$ plasma response was measured for the first time using soft x-ray cameras viewing poloidal cross-sections of the plasma at three separate toroidal locations. A model of the soft x-ray measurements was developed using the plasma response displacement calculated by MARS-F. The model, which includes no free parameters, successfully reproduces

the soft x-ray measurements over the range of β_N where MARS-F agrees with the magnetic measurements. The experiment-theory comparison of the $n=1$ plasma response revealed that although the linear ideal MHD plasma response model accurately describes the phase of the plasma response in ideal MHD stable discharges, it overestimates the amplitude as the plasma beta approaches the ideal MHD no-wall beta limit. This suggests the importance of physics absent from the linear ideal MHD model even in ideal MHD stable discharges.

Results from $n=3$ plasma response experiments and modeling underscore that there are two types of response fields: one that consists of localized currents at the rational surfaces that cancel the applied pitch resonant field and another that is excited by the components of the external field that couple to the kink mode. Both types of plasma response fields are present when external fields with strong pitch resonant components are applied to plasmas at high values of β_N . A numerical study of the $n=3$ plasma response was conducted in the parameter space relevant for ELM suppression in DIII-D. The results show the plasma response depends on both the plasma pressure and safety factor. The pressure dependence acts by changing the stability of stable kink modes and is in good agreement with the experiment. The safety factor affects the degree to which the external field couples to the kink mode and resonant field components. The resulting changes in the total non-axisymmetric field may have important consequences for understanding how ELMs are suppressed by non-axisymmetric magnetic fields.

In closing, we have discussed the wide applicability and the limitations of the linear ideal MHD plasma response model. Despite the good agreement between experiment and theory, additional internal plasma response measurements are needed to characterize the structure of non-axisymmetric plasma equilibria over a wider range of plasma conditions (particularly at low plasma rotation), to compare the effects of resonant and non-resonant magnetic fields, and to validate more complete plasma response models including plasma rotation, resistivity, and kinetic effects. These efforts would benefit greatly from local measurements of the perturbed magnetic field in the plasma. Local measurements (instead of line integrated ones) are needed to accurately measure the evolution of localized shielding currents near the rational surfaces while measurements of the magnetic field would allow the most straightforward comparison with theory.

ACKNOWLEDGMENTS

This work was supported in part by the U. S. Department of Energy under DE-FG02-04ER54761, DE-AC52-07NA27344, DE-FC02-04ER54698, DE-AC05-06OR23100, DE-FG02-08ER85196, and DE-AC02-09CH11466. The authors recognize crucial contributions from M. A. Van Zee-land concerning the development of the synthetic soft x-ray diagnostic described in this paper.

¹J. L. Luxon, T. C. Simonen, and R. D. Stambaugh, *Fusion Sci. Technol.* **48**, 807 (2005).

²G. L. Jackson, P. M. Anderson, J. Bialek, W. P. Cary, G. L. Campbell, A. M. Garofalo, R. Hatcher, A. G. Kellman, R. J. La Haye, A. Nagy, G. A.

Navratil, M. Okabayashi, C. J. Pawley, H. Reimerdes, J. T. Scoville, E. J. Strait, and D. D. Szymanski, in *Proceedings of the 30th European Physical Society Conference on Controlled Fusion and Plasma Physics, St. Petersburg, Russia*, (2003), Vol. 27A, p. 4.47.

³J. T. Scoville, R. J. La Haye, A. G. Kellman, T. H. Osborne, R. D. Stambaugh, E. J. Strait, and T. S. Taylor, *Nucl. Fusion* **31**, 875 (1991).

⁴J. L. Luxon, M. J. Schaffer, G. L. Jackson, J. A. Leuer, A. Nagy, J. T. Scoville, and E. J. Strait, *Nucl. Fusion* **43**, 1813 (2003).

⁵J.-K. Park, M. J. Schaffer, J. E. Menard, and A. H. Boozer, *Phys. Rev. Lett.* **99**, 195003 (2007).

⁶A. M. Garofalo, R. J. La Haye, and J. T. Scoville, *Nucl. Fusion* **42**, 1335 (2002).

⁷T. C. Hender, R. Fitzpatrick, A. W. Morris, P. G. Carolan, R. D. Durst, T. Edlington, J. Ferreira, S. J. Fielding, P. S. Haynes, J. Hugill, I. J. Jenkins, R. J. La Haye, B. J. Parham, D. C. Robinson, T. N. Todd, M. Valovic, and G. Vayakis, *Nucl. Fusion* **32**, 2091 (1992).

⁸T. E. Evans, R. A. Moyer, P. R. Thomas, J. G. Watkins, T. H. Osborne, J. A. Boedo, E. J. Doyle, M. E. Fenstermacher, K. H. Finken, R. J. Groebner, M. Groth, J. H. Harris, R. J. La Haye, C. J. Lasnier, S. Masuzaki, N. Ohyabu, D. G. Pretty, T. L. Rhodes, H. Reimerdes, D. L. Rudakov, M. J. Schaffer, G. Wang, and L. Zeng, *Phys. Rev. Lett.* **92**, 235003 (2004).

⁹T. E. Evans, R. A. Moyer, K. H. Burrell, M. E. Fenstermacher, I. Joseph, A. W. Leonard, T. H. Osborne, G. D. Porter, M. J. Schaffer, P. B. Snyder, P. R. Thomas, J. G. Watkins, and W. P. West, *Nat. Phys.* **2**, 419 (2006).

¹⁰A. Garofalo, W. Solomon, M. Lanctot, K. Burrell, J. DeBoo, J. deGrassie, G. Jackson, J.-K. Park, H. Reimerdes, M. Schaffer, and E. Strait, *Phys. Plasmas* **16**, 056119 (2009).

¹¹H. E. Mynick, *Phys. Plasmas* **13**, 058102 (2006).

¹²J. Freidberg, *Ideal Magnetohydrodynamics* (Plenum, New York, 1987).

¹³A. H. Boozer, *Phys. Plasmas* **6**, 831 (1999).

¹⁴A. H. Boozer, *Phys. Rev. Lett.* **86**, 5059 (2001).

¹⁵L. L. Lao, H. E. St. John, Q. Peng, J. R. Ferron, E. J. Strait, T. S. Taylor, W. H. Meyer, C. Zhang, and K. I. You, *Fusion Sci. Technol.* **48**, 968 (2005).

¹⁶Y. Q. Liu, A. Bondeson, C. M. Fransson, B. Lennartson, and C. Bretholtz, *Phys. Plasmas* **7**, 3681 (2000).

¹⁷J.-K. Park, A. H. Boozer, and A. H. Glasser, *Phys. Plasmas* **14**, 052110 (2007).

¹⁸A. M. Garofalo, T. H. Jensen, and E. J. Strait, *Phys. Plasmas* **10**, 4776 (2003).

¹⁹H. Reimerdes, M. S. Chu, A. M. Garofalo, G. L. Jackson, R. J. La Haye, G. A. Navratil, M. Okabayashi, J. T. Scoville, and E. J. Strait, *Phys. Rev. Lett.* **93**, 135002 (2004).

²⁰H. Grad, *Ann. N.Y. Acad. Sci.* **357**, 223 (1980).

²¹R. T. Snider, R. Evanko, and J. Haskovec, *Rev. Sci. Instrum.* **59**, 1807 (1988).

²²H. Reimerdes, J. Bialek, M. S. Chance, M. S. Chu, A. M. Garofalo, P. Gohil, Y. In, G. L. Jackson, R. J. Jayakumar, T. H. Jensen, J. S. Kim, R. J. La Haye, Y. Q. Liu, J. E. Menard, G. A. Navratil, M. Okabayashi, J. T. Scoville, E. J. Strait, D. D. Szymanski, and H. Takahashi, *Nucl. Fusion* **45**, 368 (2005).

²³H. Reimerdes, A. M. Garofalo, E. J. Strait, R. J. Buttery, M. S. Chu, Y. In, G. L. Jackson, R. J. La Haye, M. J. Lanctot, Y. Q. Liu, M. Okabayashi, J.-K. Park, M. J. Schaffer, and W. M. Solomon, *Nucl. Fusion* **49**, 115001 (2009).

²⁴R. Fitzpatrick, *Nucl. Fusion* **33**, 1049 (1993).

²⁵M. J. Lanctot, H. Reimerdes, A. M. Garofalo, M. S. Chu, Y. Q. Liu, E. J. Strait, G. L. Jackson, R. J. La Haye, M. Okabayashi, T. H. Osborne, and M. J. Schaffer, *Phys. Plasmas* **17**, 030701 (2010).

²⁶C. T. Holcomb, M. A. Makowski, R. J. Jayakumar, S. A. Allen, R. M. Ellis, R. Geer, D. Behne, K. L. Morris, L. G. Seppala, and J. M. Moller, *Rev. Sci. Instrum.* **77**, 10E506 (2006).

²⁷T. N. Carlstrom, G. L. Campbell, J. C. DeBoo, R. Evanko, C. M. Greenfield, J. Haskovec, C. L. Hsieh, E. McKee, R. T. Snider, R. Stockdale, P. K. Trost, and M. P. Thomas, *Rev. Sci. Instrum.* **63**, 4901 (1992).

²⁸K. H. Burrell, D. H. Kaplan, P. Gohil, D. G. Nilson, R. J. Groebner, and D. M. Thomas, *Rev. Sci. Instrum.* **72**, 1028 (2001).

²⁹H. E. St. John, J. R. Ferron, L. L. Lao, T. H. Osborne, S. J. Thompson, and D. Wroblewski, in *Proceedings of the 15th International Conference on Plasma Physics and Controlled Nuclear Fusion Research, Seville, Spain* (1994), Vol. 3, p. 603.

³⁰H. Reimerdes, J. W. Berkery, M. J. Lanctot, A. M. Garofalo, J. M. Hanson, Y. In, R. J. La Haye, M. Okabayashi, S. A. Sabbagh, and E. J. Strait, "Evidence for the importance of trapped particle resonances for resistive

- wall mode stability in high beta tokamak plasmas,” *Phys. Rev. Lett.* **106**, 215002 (2011).
- ³¹I. N. Bogatu, D. H. Edgell, and J.-S. Kim, *Rev. Sci. Instrum.* **75**, 2832 (2004).
- ³²C. Chantler, X-ray form factor, attenuation, and scattering tables (2005), <http://www.nist.gov/physlab/data/ffast/index.cfm>.
- ³³M. J. Schaffer, J. E. Menard, M. P. Aldan, J. Bialek, T. E. Evans, and R. A. Moyer, *Nucl. Fusion* **48**, 024004 (2008).
- ³⁴D. Pfirsch and H. Tasso, *Nucl. Fusion* **11**, 259 (1971).
- ³⁵M. S. Chu, M. S. Chance, A. H. Glasser, and M. Okabayashi, *Nucl. Fusion* **43**, 441 (2003).
- ³⁶J. Crotinger, “Corsica: A comprehensive simulation of toroidal magnetic-fusion devices,” Lawrence Livermore National Laboratory Technical Report UCRL-ID-126284 (1997).
- ³⁷E. J. Strait, *Fusion Sci. Technol.* **48**, 864 (2005).
- ³⁸K. H. Burrell, T. E. Evans, E. J. Doyle, M. E. Fenstermacher, R. J. Groebner, A. W. Leonard, R. A. Moyer, T. H. Osborne, M. J. Schaffer, P. B. Snyder, P. R. Thomas, W. P. West, J. A. Boedo, A. M. Garofalo, P. Gohil, G. L. Jackson, R. J. La Haye, C. J. Lasnier, H. Reimerdes, T. L. Rhodes, J. T. Scoville, W. M. Solomon, D. M. Thomas, G. Wang, J. G. Watkins, and L. Zeng, *Plasma Phys. Controlled Fusion* **47**, B37 (2005).